CORRESPONDENCE OF A GLOBAL ISOLATED SUBSTORM TO THE MCPHERRON STATISTICAL MODEL

V.A. Parkhomov (iD)
Baikal State University,
Irkutsk, Russia, pekines_41@mail.ru

V.G. Eselevich (iD)
Institute of Solar-Terrestrial Physics SB RAS,
Irkutsk, Russia, esel@iszf.irk.ru

M.V. Eselevich (iD)
Institute of Solar-Terrestrial Physics SB RAS,
Irkutsk, Russia, mesel@iszf.irk.ru

B. Tsegmed (iD)
Institute of Astronomy and Geophysics MAS,
Ulaanbaatar, Mongolia, tseg@iag.ac.mn

S.Yu. Khomutov (iD)
Institute of Cosmophysical Research
and Radio Wave Propagation FEB RAS,
Paratunka, Russia, khomutov@ikir.ru

T. Raita (iD)
Sodankylä Geophysical Observatory, University of Oulu,
Sodankylä, Finland, tero.raita@sgo.fi

G.V. Popov
Baikal State University,
Irkutsk, Russia, popov2898@mail.ru

A.A. Mochalov
Polar Geophysical Institute RAS,
Apatity, Russia, mochalov@pgia.ru

S.V. Pilgaev
Polar Geophysical Institute RAS,
Apatity, Russia, pilgaev@pgia.ru

†R.A. Rakhmatulin
Institute of Solar-Terrestrial Physics SB RAS,
Irkutsk, Russia

Abstract. It is shown that a diamagnetic structure (DS) of the slow solar wind (SW), the source of which on the Sun was a chain of streamers, arrived at Earth's orbit on December 22, 2015. It interacted with Earth's magnetosphere under conditions when the northward B_z component of the interplanetary magnetic field (IMF) remained for a long time in preceding undisturbed SW. The interaction and a sharp change in the direction of B_z to the south generated an isolated substorm whose duration depends on the duration of interaction with the DS. The substorm began at midday with the passage of the DS into the magnetosphere and spread to the east. All phases of the substorm — growth, expansion, and recovery — were observed for two hours. Variations in the SW and IMF parameters are shown to coincide for the isolated substorm whose energy source was the slow solar wind DS, and a trigger was the abrupt change in the direction of the vertical IMF component from north to south. The coincidence is justified by statistical generalizations of the same parameters in 40 % of cases of long-term observations of individual substorms whose trigger was a change in B_z direction.

Keywords: diamagnetic structure, global isolated substorm, change in the B_z direction, trigger.

INTRODUCTION

One of the main questions faced by magnetospheric physics about factors that control the energy input to the magnetosphere and the intensity of substorms remains open. It has been established that the energy sources of magnetospheric substorms are solar wind (SW) plasma and the interplanetary magnetic field (IMF). The most common point of view is that the main parameters determining the accumulation of energy in the magnetotail, which is released during substorms, are IMF and its B_z component. The solar wind parameters such as SW plasma velocity and density are not considered separately as energy sources for substorm disturbances, but are included in various composite indices [Akasofu, 2017; Kepko et al., 2015; Vorobjev et al., 2018; Troshichev, Janzhura, 2012].

In [Lemaire, Roth, 1981; Pneuman, 1983; Karlsson et al., 2015], the concept of plasmoids in SW was introduced. Such structures are defined in [Eselevich, Eselevich, 2005; Parkhomov et al., 2018] as plasma diamagnetic structures (DS). Collision of slow-SW diamagnetic structures with the magnetosphere can cause substorm-like magnetospheric disturbances, in particular so-called sawtooth substorms. In [Eselevich, Eselevich, 2005; Parkhomov et al., 2018; Parkhomov et al., 2015, 2020], the diamagnetic structures that are seen near the Sun as higher brightness rays are shown to form the basis of slow quasi-stationary SW in Earth's orbit. Solar sources of slow quasi-stationary SW are the streamer belt [Svalgaard et al., 1974; Eselevich et al., 1999] and streamer chains [Eselevich et al., 1999] or pseudostreamers [Wang et al., 2007]. In Earth's orbit, slow SW features a higher plasma density $N>10\pm2$ cm^{-3} and a relatively low velocity $V\approx250$–450 km/s as compared to fast SW flowing from coronal holes at $V\approx450$–800 km/s [Borrini et al., 1981; Eselevich, Fainshtein 1991].

Both the streamer chains in the corona and the streamer belt look in white light as a sequence of higher brightness rays (plasma density), and slow SW with approximately the same properties flows in them. None-

theless, the chains differ from the belt in that they separate coronal regions with open magnetic field lines having the same polarity [Svalgaard et al., 1974].

In this case, the higher brightness rays in the streamer chains, as well as those in the streamer belt, are quasi-stationary diamagnetic structures of slow SW, which are defined by the presence of a negative correlation coefficient between SW density N and IMF modulus B jumps.

This paper is a sequel to the research into the nature of the global magnetospheric disturbance associated with the December 22, 2015 impact of DS from a streamer chain on Earth's magnetosphere. This diamagnetic structure (hereinafter referred to as December 22, 2015 DS) generated a global magnetospheric disturbance in the form of a powerful isolated substorm (AE_{max}=1076 nT) and a weak magnetic storm ($SYM\text{-}H_{max}$=–37 nT).

1.   DATA AND METHODS

In the first part of the paper, we identify the December 22, 2015 DS source on the Sun, and then trace the dynamics of the DS in the solar wind and magnetosphere from ACE, Wind, THEMIS, GOES-13, GOES-15, RPSB A, B (Van Allen) satellite observations. We analyze the magnetospheric response, using data from the ground-based magnetometer networks INTERMAGNET, CARISMA, IMAGE and induction magnetometers of Ivalo, Borok, Lovozero, Mondy, Istok, and Paratunka observatories. Details of the terrestrial response are studied from observations on three meridians — noon, dusk, and midnight. As geomagnetic activity indices we use auroral activity indices: the global index SML determined from geomagnetic field measurements made at the global network of 300 SuperMag observatories [Gjerloev, 2012], the local index *IL* determined from geomagnetic field variations at the meridional IMAGE magnetometer network [https://space.fmi.fi/image/www/index.php?page=il_index], and the *CL* index determined from observations at the Canadian magnetometer network CARISMA [http://carisma.ca/carisma-data/fgm -auroral-indices].

The list and location of the satellites whose data are used are given in Figures 1, 2 and in Table 1; the list of observatories, in Table 2.

We are interested in the December 22, 2015 DS, presented in Figure 3 as variations in the IMF components B, B_y, B_z, SW plasma parameters V, N, P, and geomagnetic activity indices AL and $SYM\text{-}H$ derived from OMNI data [http://cdaweb.gsfc.nasa.gov/cgi-bin/eval2.cgi]. The vertical rectangle for the time interval ≈09:00–12:00 UT marks the DS that was determined from the anticorrelation between plasma density N and IMF modulus B. The DS caused a magnetospheric disturbance in the form of an isolated substorm (AL_{max}=1076 nT), observed during the decay phase of a large magnetic storm on December 20, 2015 Dst_{max} =155 nT at 23:00 UT [http://wdc.kugi.kyoto-u.ac .jp/dst_provisional/201512/index.html]. Let us provide evidence for the isolation and global nature of the substorm caused by this DS. Despite significant variations in the SW and IMF parameters for seven hours before the onset of the DS related substorm, average auroral

activity indices change insignificantly (AE_{av}=136.2±3.4 nT, AL_{av}=−50.4±2.8 nT) and there are no substorms except for that under study (see Figure 3). Thus, according
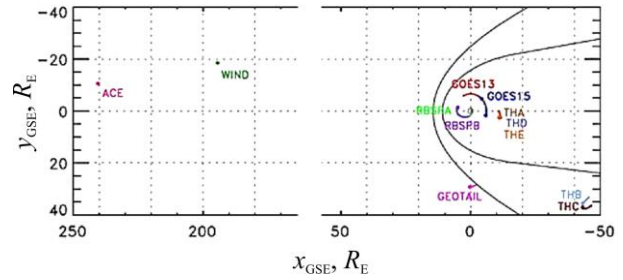

Figure 1. Location of satellites in the magnetosphere in GSE coordinates in the XY plane from 09:00 to 13:00 UT on December 22, 2015. Dots indicate the beginning of motion
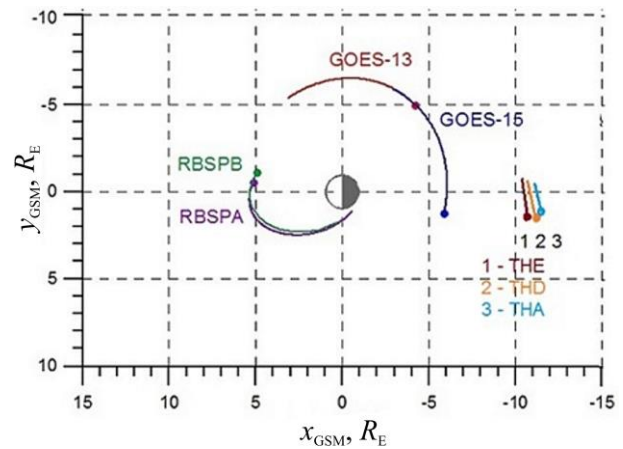

Figure 2. Location of satellites in the magnetosphere in GSM coordinates in the XY plane from 09:00 to 13:00 UT
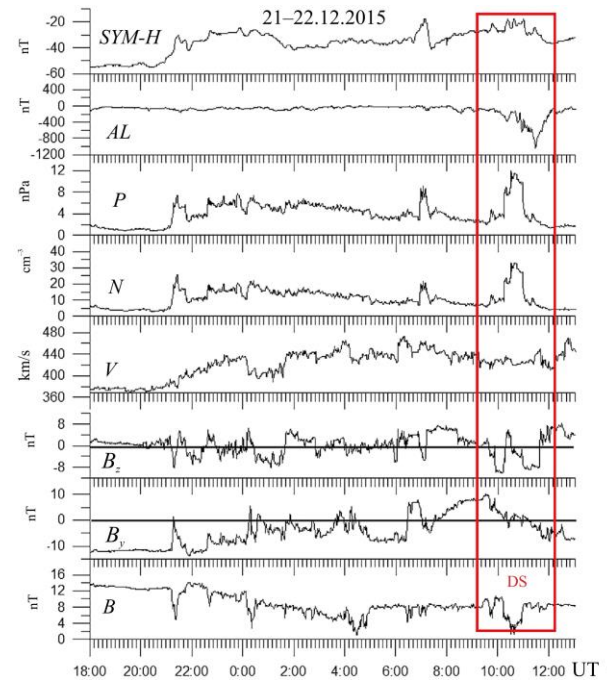

Figure 3. Variations in the IMF components B, B_y, B_z, SW plasma parameters V, N, P, and geomagnetic activity indices AL and $SYM\text{-}H$ as derived from OMNI data [http://cdaweb.gsfc.nasa.gov/cgi-bin/eval2.cgi]. The rectangle marks DS

V.A. Parkhomov, V.G. Eselevich, M.V. Eselevich, B. Tsegmed, S.Yu. Khomutov, Tero Raita, G.V. Popov, A.A. Mochalov,
S.V. Pilgaev, R.A. Rakhmatulin

Satellite coordinates at 09:40 UT

No.	Satellite	x_{GSM}, R_E	y_{GSM}, R_E	z_{GSM}, R_E	R, R_E
1	ACE	239.89	−10.57	24.62	241.38
2	Wind	194.42	−18.66	−11.19	195.63
3	THA	11.52	1.40	−3.47	12.11
4	THB	−4.32	35.59	−4.22	36.10
5	THC	−4.32	37.00	−3.68	37.43
6	THD	−11.95	1.32	−4.41	12.80
7	THE	−11.37	1.37	−4.00	12.13
8	Geotail	−0.24	29.16	1.83	29.22
9	GOES-13	−2.99	−6.08	−0.50	6.80
10	GOES-15	−5.99	1.00	−2.60	6.61
11	RPSB-A	3.54	4.41	0.13	5.66
12	RPSB-B	4.00	3.98	0.20	5.65

No.	Station name and abbreviation	Geomagnetic coordinates, deg.		Local geomagnetic time, hr.	Meridional chain	Type of magnetometer and sample rate
		N	E			
1	Lovozero (LOZ)	63.5	126.8	UT+2	IMAGE	induction, 40 Hz
2	Borok (BOR)	53.6	123.6	UT+2	IPE	induction, 10 Hz
3	Istok (IST)	60.1	166.5	UT+6	ISTP	induction, 64 Hz
4	Mondy (MND)	42.5	177.5	UT+7	ISTP	induction, 64 Hz
5	Paratunka (PET)	46.3	222.6	UT+11	IKIR	induction, 64 Hz
6	Ministik Lake (MSTK)	60.1	309.1	UT−8.1	CARISMA	induction, 20 Hz
7	Fort Churchill (FCHU, FCC)	67.4	330.3	UT−6.4	CARISMA	induction, 20 Hz fluxgate, 1 Hz
8	Ivalo (IVA)	65.1	121.1	UT+2	IMAGE	induction, 40 Hz
9	I. Vize (VIZ)	70.4	163.5	UT+6	AARI	fluxgate, 0.0166 Hz
10	Pebek (PBK)	70.83	170.90	UT+11	AARI	fluxgate, 0.0166 Hz
11	Tamanrasset (TAM)	24.45	82.30	UT+1	INTERMAGNET	fluxgate, 0.0166 Hz
12	Hyderabad (HYB)	8.84	152.23	UT+6	INTERMAGNET	fluxgate, 0.0166 Hz
13	Guam (GUA)	5.80	216.49	UT+9.6	INTERMAGNET	fluxgate, 0.0166 Hz
14	San Juan (SJG)	27.78	6.94	UT−4	INTERMAGNET	fluxgate, 0.0166 Hz

to the algorithm for determining isolation [Vorobjev et al., 2018], the substorm is isolated. The global nature in the magnetic activity indices *SML*, *CL*, *IL*, and the *H* component in auroral and low-latitude observatories (see below Figure 6).

2. IDENTIFICATION OF DS IN EARTH'S ORBIT ON DECEMBER 22, 2015 AND ITS SOLAR SOURCE

Let us locate the solar source of this DS and analyze the events, which preceded its occurrence in Earth's orbit, at a distance of 1 AU. For this purpose, we present data on IMF and SW (see Figure 3) for a longer time interval December 16–23, 2015 (Figure 4). From Figure 4 follows that there was a shock wave (December 19, 2015, ~16:05 UT) before the appearance of the DS, which corresponds to SSC [http://www.obsebre.es/en/rapid], and a region of shock-heated plasma and a magnetic cloud, or interplanetary coronal mass ejection (ICME), behind it. The velocity of the shock front at a distance of 1 AU $Vs \approx 470$ km/s. According to [Eselevich, 1990], the time of passage Δt of such a front from the Sun to Earth can be estimated from the formula

$$\Delta t \approx 215 R_\odot / (1.5 V), \qquad (1)$$

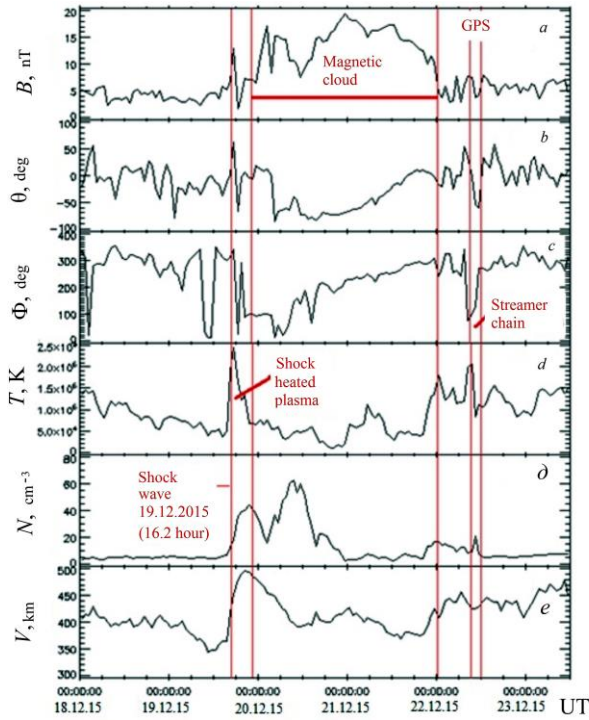where $R_\odot \approx 6.9 \cdot 10^6$ km is the solar radius.

39

Figure 4. Parameters of the interplanetary magnetic field and solar wind plasma: IMF modulus (*a*); IMF longitude angle θ (*b*); IMF azimuth angle Φ (*c*); SW plasma temperature *T* (*d*); plasma density *N* (*e*); SW velocity *V* (*f*). Parts of the streamer belt in Earth's orbit and the heliospheric plasma sheet (HPS) are indicated by vertical lines. According to OMNI data [http://cdaweb.gsfc.nasa.gov/cgi-bin/eval2.cgi]

For $V_s \approx 470$ km/s Formula (1) yields $\Delta t \approx 2$ days 10 hrs. Hence it follows that the coronal mass ejection (CME) that produced the ICME and the shock wave emerged on the Sun on December 17, 2015 at ≈16:00 UT. According to the CME catalog [https://cdaw.gsfc.nasa.gov/CME_list], the closest halo-type CME in terms of time and maximum velocity occurred on the

Sun at a point with coordinates S13W04 on December 16, 2015 at ~09:36 UT and was accompanied by a C7 X-ray flare. Its initial radial velocity V_0 is estimated from the relation [Schwenn et al., 2005]: $V_0 \approx V_e / 0.88 = 740$ km/s, where $V_e \approx 650$ km/s is the maximum velocity of the halo CME in the plane of the sky near the Sun [https://cdaw.gsfc.nasa.gov/ CME_list].

Obviously, accurate within 24 hours this CME is the only possible source of the shock wave and ICME considered at a distance of 1 AU since in December 2015 there were no more such fast halo CMEs for at least a week [https://cdaw.gsfc.nasa.gov/CME_list].

Referring to Figure 4, the December 22, 2015 DS arrived at a distance of 1 AU when all these events were over. The question arises about its solar source. Before answering this question, note that according to Figure 4 this DS has the following features:

1) higher plasma density $N \approx 30$–35 cm^{-3};
2) low SW velocity $V \approx 430$ km/s;
3) presence of an even number of IMF sign changes within its limits since the azimuth angle Φ changes approximately by 180° (from ≈320° to ≈140°) and vice versa, i.e. the IMF sign changes first from "–" (sunward) to "+" (antisunward), and then back.

Such features are typical of SW streams outflowing from streamer chains [Eselevich et al., 2007]. To identify the solar source of the December 22, 2015 DS, turn to Figure 5. This figure, according to calculations made by G.V. Rudenko [http://bdm.iszf.irk.ru] in the potential approximation for ~20:31 UT on December 15, 2015, locates footpoints of open magnetic tubes corresponding to coronal holes in spherical coordinates (*a*) and presents a synoptic map of the Carrington revolution CR2171 (*b*). We are interested in the segment of intersection of the streamer chain (dashed curve) with the ecliptic marked with the letter "O" on the synoptic map in Figure 5, *b* (near longitude ≈112°) and with a vertical arrow. The streamer chain considered separates footpoints of the coronal holes denoted by a and b in Figure 5, *a*.
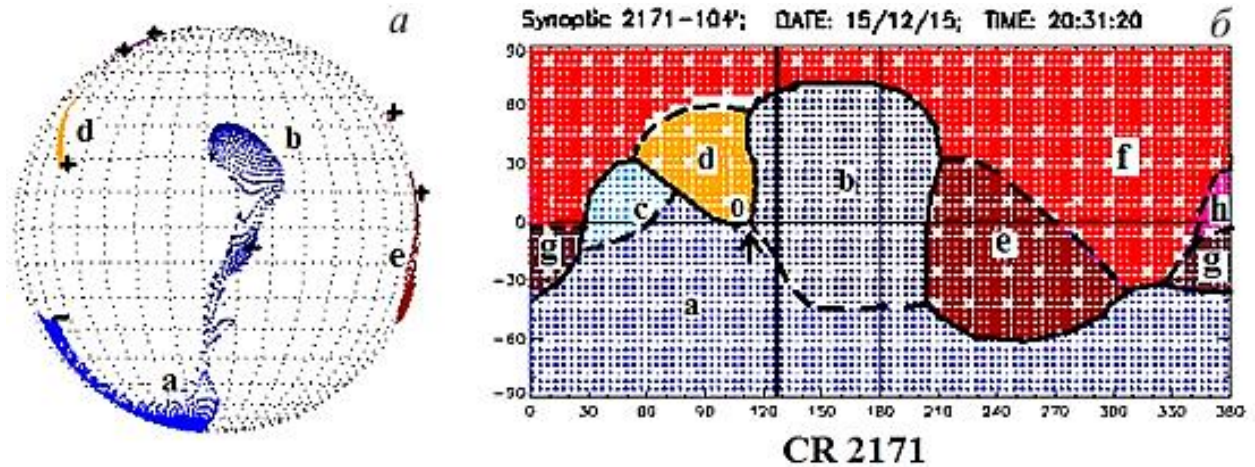

Figure 5. Results of calculations made by Rudenko G.V. [http://bdm. iszf.irk.ru] in the potential approximation for December 15, 2015 (~20:31 UT) of: (*a*) locations of footpoints of open magnetic tubes corresponding to coronal holes in spherical coordinates ("+" is the antisunward magnetic field polarity; "–" is the sunward one); *b* — a synoptic map of the Carrington revolution CR2171, which shows location of the neutral line (solid curve) and streamer chains (dashes) on the source surface ($R = 2.5 R_\odot$); the thick vertical line marks the location of the central meridian for December 15, 2015 (~22:31 UT). Different colors and Latin letters a–h indicate regions of the radial magnetic field from various coronal holes.

V.A. Parkhomov, V.G. Eselevich, M.V. Eselevich, B. Tsegmed, S.Yu. Khomutov, Tero Raita, G.V. Popov, A.A. Mochalov, S.V. Pilgaev, R.A. Rakhmatulin

Location of the central meridian at ~20:31 UT on December 15, 2015 is indicated by the vertical thick line in Figure 5, *b*. Due to solar rotation, as shown in Figure 5, *b*, the point O crosses the central meridian when it shifts to the left in longitude by ~15°, which corresponds to a time interval of ~1 day 3 hrs (rotation by 13.3° per day), i.e. on December 17, 2020 at $t_0 \approx 00{:}00$ UT the point O is on the central meridian. In Earth's orbit, an SW region with an even number of changes of IMF azimuth angle sign, a higher plasma density $N \approx 30$–35 cm^{-3}, and a relatively low velocity $V \approx 430$ km/s was observed on December 22, 2015 from 08:00 to 12:00 UT (see Figure 5). This is the DS we are interested in. Using the formula $t_{\text{Earth}} \approx [t_0 + 4.6 \cdot 10^4 / V]$ from [Eselevich et al., 2007], we can estimate the time of arrival of a plasmoid at Earth's orbit, which is a continuation of the segment O of the streamer chain crossing the central meridian in Figure 5, *b* at $t_0 \approx 00{:}00$ UT on December 17, 2020, assuming that $V \approx 430$ km/s: $\Delta t_{\text{Earth}} \approx 4.6 \cdot 10^4 / V \approx 107$ hrs ≈ 4 days 11 hrs. Hence, $t_{\text{Earth}} \approx$ December 21, 2015 (11:00 UT). This agrees up to ≈ 1 day with the time of DS appearance at a distance of 1 AU on December 22, 2015 (08:00–12:00 UT).

Thus, we come to the conclusion that the solar source of the DS recorded on December 22, 2015 (08:00–12:00 UT) is a streamer chain.

The diamagnetic structure moves toward Earth's orbit at a slow SW velocity of 430 km/s and has a number of features. First of all, for ~4.5 hrs (05:00–09:36 UT) the IMF vertical component has predominantly northward direction and an average value of 2.3 nT, whereas from 07:10 to 09:36 UT the average value of B_z is 6.1 nT. It is significant that the IMF components B_y and B_x are also positive. These facts indicate that there is no energy accumulation in the magnetosphere due to reconnection of the magnetospheric magnetic field and IMF.

The mean SW plasma density from 07:10 to 09:40 UT was $N = 8.4$ cm^{-3}. At 09:40 UT there was a density jump to $N \approx 13$ cm^{-3}; at 10:13 UT the density increased to ~21 cm^{-3}, and at 10:40 UT it reached its maximum value of 33 cm^{-3}. Specifically, the IMF modulus varies in antiphase with the density ($r = -0.74$), which, as noted above, is an indication of the diamagnetic structure [Parkhomov et al., 2018].

3. GLOBAL GEOMAGNETIC RESPONSE OF THE MAGNETOSPHERE TO INTERACTION WITH THE DECEMBER 22, 2015 DS

Let us examine the geomagnetic response to the DS–magnetosphere interaction in *SML*, *IL*, and *CL* variations (Figure 6, *a*, *e*), in longitudinal features of geomagnetic pulsations (Figure 6, *f*), and in variations of the horizontal component of the geomagnetic field (see Figure 6, *g*). According to [Gjerloev, 2012], the substorm began at 10:14 UT (arrow 1 in Figure 6, *a*, *e*). However, as inferred from *IL*-index variations (Figure 6, *a*, *e*, blue curves), the onset of the substorm can be detected at ~09:38 UT. At the same time, B_z changes sign (marked off by the vertical red line), which suggests activation of a trigger that provides energy inflow into the magnetosphere. According to variations of the indices, we can recognize three substorm phases (designated as I, II, III). During the first phase, 09:38–10:14 UT, variations in the *IL* index from –0 to –60 nT (Figure 6, *a*, *e*, blue curves), in the *CL* index from –50 to –80 nT (Figure 6, *e*, red curve), and in the *SML* index from –230 to –400 nT (Figure 6, *a*, red curve) coincide with a change in Bz from 0 to –10 nT (Figure 6, *b*) and an increase in the SW plasma density from 5 to 10.6 cm^{-3} (Figure 6, *c*). The second substorm phase begins with a plasma density jump from 9 to 31 cm^{-3}, a decrease in the IMF modulus from 11 to 5 nT, and a change in B_z from –10 to +10 nT. This moment coincides with the moment of the substorm onset at 10:14 UT determined in [Gjerloev, 2012]. During the substorm expansion phase from 10:55 UT, all the indices vary synchronously with two simultaneous extremes of *SML*, *IL*, and *CL* observed at 11:00 and 11:27 UT. At 11:30 UT, the recovery phase begins — a weakening of the intensity of ionospheric currents and recovery of all the indices to the undisturbed level. This regularity points to a common global cause of the auroral electrojet modulation. This cause is the interaction between the magnetosphere and the DS characterized by variations in the SW density and the IMF vertical component B_z. Duration of the substorm and its energy depend on the duration (the horizontal red straight line in Figure 6) of the DS–magnetosphere interaction or on the influx of SW energy carried by the DS into the magnetosphere. The energy inflow is, however, controlled by the variation of the IMF vertical component B_z.

Calculate the energy E_{kin} carried by the DS into the magnetosphere on December 22, 2015 for $\Delta t \approx 40$ min (2400 s) from 10:15 to 10:55 UT. Average SW parameters for this interval: $N \approx 25$ cm^{-3}, $V_{\text{sw}} \approx 430$ km/s. The DS diameter: $d \approx \Delta t V_{\text{sw}} \approx 2400 \cdot 430 \approx 1.03 \cdot 10^6$ km. The DS sectional area: $S \approx \pi d^2 / 4 \approx 8.4 \cdot 10^{11}$ km^2.

Length of the DS affecting the magnetosphere: $L \approx 30 R_{\text{E}} \approx 1.9 \cdot 10^5$ km.

We obtain the volume of the structure: $SL \approx 1.6 \cdot 10^{17}$ km^3 (~$1.6 \cdot 10^{32}$ cm^3).

$$E_{\text{кин}} = N m_{\text{p}} V_{\text{sw}}^2$$

$E_{\text{kin}} = N m_{\text{p}} V_{\text{sw}}^2 SL \approx 6.14 \cdot 10^{24}$ erg ($6.14 \cdot 10^{14}$ J).

This value is comparable with the estimates of energy release during substorms in "Short-Term Space Weather Forecast" by IKI RAS [http://spaceweather.ru/ru/node/32]. To estimate the energy supplied to the magnetosphere for 90 min, we use the parameter $\varepsilon = 2 \cdot 10^7 V_{\text{i}} B^2 \sin(\theta/2)^4$ [W], where B is the magnetic field in nT; V_{i} is the solar wind speed in km/s; θ is the IMF hour angle in the YZ plane. As estimated [http://spaceweather.ru/ru/node/32], $E_{90} < 10^{14}$ J enters the magnetosphere for 90 min at the level "quiet", and $E_{90} = 10^{14} \div 10^{15}$ J at the level "weak substorms", which is comparable to the December 22, 2015 DS energy.

Examine the features of geomagnetic pulsations from noon to midnight and morning hours since the ultralow-frequency radiation, which they reflect, serves as a good indicator of magnetospheric processes associated with substorms [Saito, 1969; Nishida, 1980;
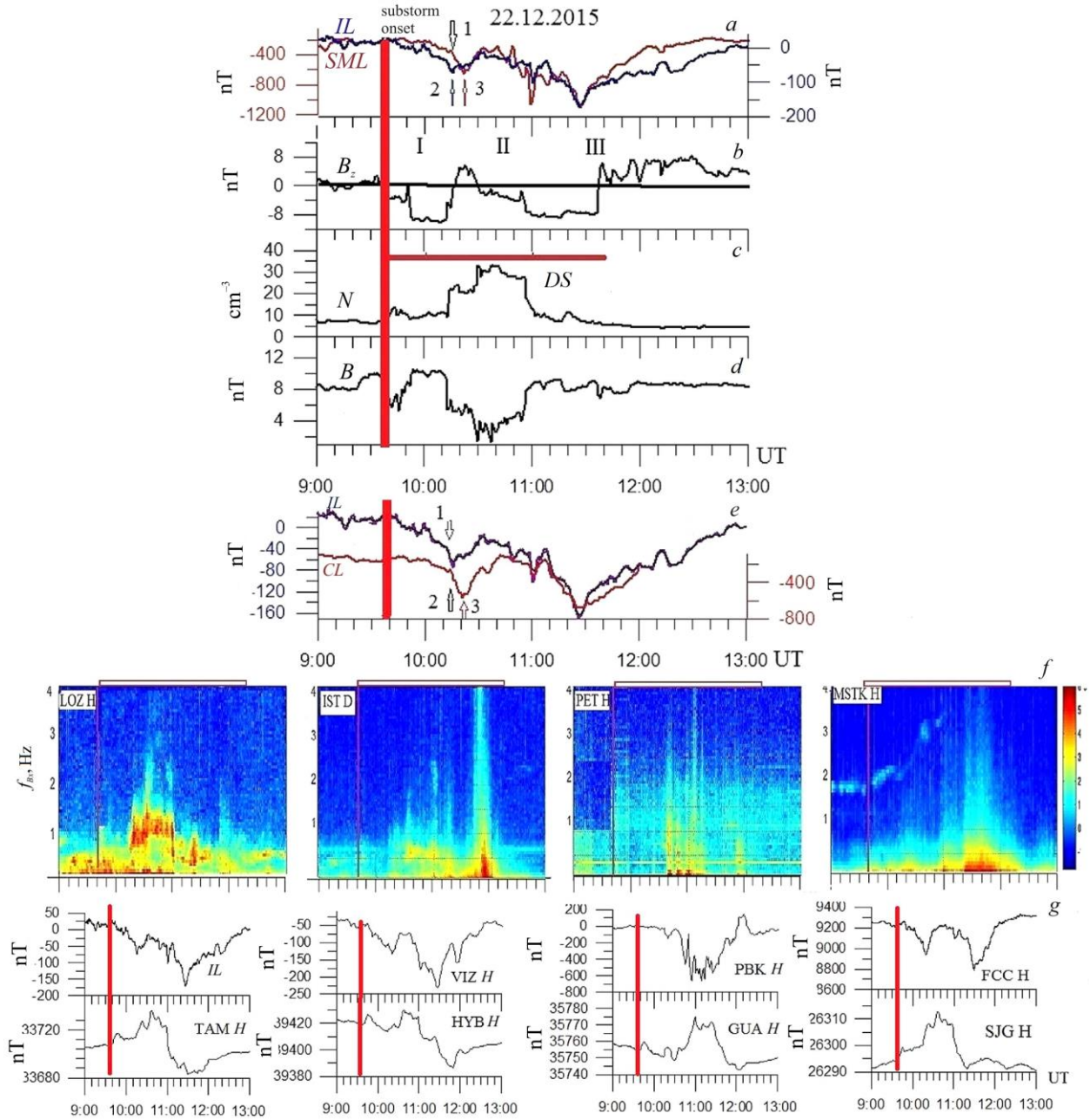
Figure 6. Variations in the *SML* and *IL* indices (*a*), IMF B_z (*b*), SW density (*c*), IMF intensity modulus measured by Wind (*d*), *IL* and *CL* indices (*e*), spectrograms of geomagnetic pulsations in different longitudinal sectors (*f*), magnetograms from auroral and low-latitude observatories in one longitude interval corresponding to the longitudes of the observatories in which the spectrograms were obtained (*g*). The horizontal rectangle denotes DS. The solid vertical line is the beginning of interaction with the DS. Arrows show: 1— the substorm onset according to [Gjerloev, 2012]; 2 and 3 — maxima in the absolute value of the *IL* and *CL* indices respectively. Roman numerals denote the substorm phases: I — growth; II — expansion; III —recovery

Kangas et al., 1998]. In the near noon sector, pulsations are observed in the Pc1 frequency range with a nonstationary spectrum (Figure 6, *f*, LOZ *H*), which are accompanied by an increase in the westward current reflected in an increase in the *IL* index to –200 nT (Figure 6, *e*), determined from *H*-component variations at the meridional magnetometer network IMAGE. To the east in the dusk sector 16–18 MLT, there is a short-term intensification of auroral current (negative bay ~–600 nT in Figure 6, *g*, VIZ *H*) and a broadband burst of Pi1-2 pulsations at ~10:20 UT (Figure 6, *e*, IST *D*). In the midnight sector (21–23 MLT, PBK), the intensity of the

westward electrojet sharply increases ($H \sim$–700 nT); at the mid-latitude station PET of this meridian there are successive broadband Pi1-2 bursts typical for the substorm growth phase (Figure 6, *f*, *g*) [Rakhmatulin et al., 1984; Karlsson et al., 2015]. In the post-midnight sector 02–06 MLT, the common phenomena constituting a substorm are observed: a powerful westward current (H=–500 nT), PiC pulsations typical of the substorm recovery phase (at the MSTK, FCC observatories of the CARISMA network). The change in modes and types of the geomagnetic pulsations along the longitude reflects the dynamics of the DS — magnetosphere interaction

V.A. Parkhomov, V.G. Eselevich, M.V. Eselevich, B. Tsegmed, S.Yu. Khomutov, Tero Raita, G.V. Popov, A.A. Mochalov,
S.V. Pilgaev, R.A. Rakhmatulin

and shows that pulsations of different types are excited simultaneously, which, in turn, points to various mechanisms of MHD wave generation. In addition, there is a delay in the ionospheric current amplification maxima to the east of the noon meridian (see Figure 6, arrows 2, 3). These regularities of the change in pulsation modes along the longitude do not fit into the existing models of generation of geomagnetic pulsations accompanying a substorm and contradict the classical results [Akasofu, 2017; Kepko et al., 2015]. All classical models of magnetospheric substorm onset include the main elements of substorm current wedge, which moves westward of the midnight meridian and provides conditions for the interaction between the magnetospheric reconfiguration and the ionosphere dynamics.

The differences between the isolated global substorm considered and the classical substorm are also confirmed by Figure 7, *a–f*, which presents SW and IMF parameters, spectrograms of geomagnetic pulsations at Ivalo (low-frequency part of the spectrum 0.022–0.0045 Hz) and Lovozero (high-frequency part 0.1–4 Hz) observatories, variations in partial density of protons inside the magnetosphere at a distance of $\sim 5R_E$ obtained by the RBSPA satellite, and an oscillogram of geomagnetic pulsations filtered in a particular range 0.1–5 Hz at Ivalo Observatory. Referring to Figure 7, *c*, in the low-frequency part of the spectrum are bursts (indicated by vertical segments) of Pi2 pulsations with an average period $T\sim 150$ s. Recall that the Pi2 pulsations are a generally recognized indicator of substorm onset. However, the situation considered develops during the near noon hours at subauroral latitudes. Each burst is seen to coincide with the moment of transition of B_z through 0 and with sharp peaks of B_z.

This suggests a separate effect of IMF changes and proton density jumps on the mode of geomagnetic pulsations. Bursts of Pi2 pulsations are associated with the sharp change in the direction of B_z from north to south or vice versa, presumably due to the reconnection between IMF and the geomagnetic field at the magnetopause, the generation of jets in the magnetosheath, and their impulsive passage into the magnetosphere. A similar regularity was first discovered in [Dmitriev, Suvorova, 2015] and noted by us in [Parkhomov et al., 2021], where it was shown that Pc4–5 – Pi2 bursts (100–200 s) may be driven by the passage of MHD waves from SW into the magnetosphere when DS penetrates into the magnetosheath. Confirmation of this assumption can be found in [Katsavriasi et al., 2021], where Pi2 pulsations are shown to occur in the magnetosheath and with a delay of 140 s inside the magnetosphere, which, according to the authors, is associated with the Alfvén velocity and the wave transmission through the magnetopause. As we noted in [Parkhomov et al., 2021], a possible mechanism for the wave transmission through the magnetopause may be the impulsive passage according to the mechanism [Echim, Lemaire, 2000].

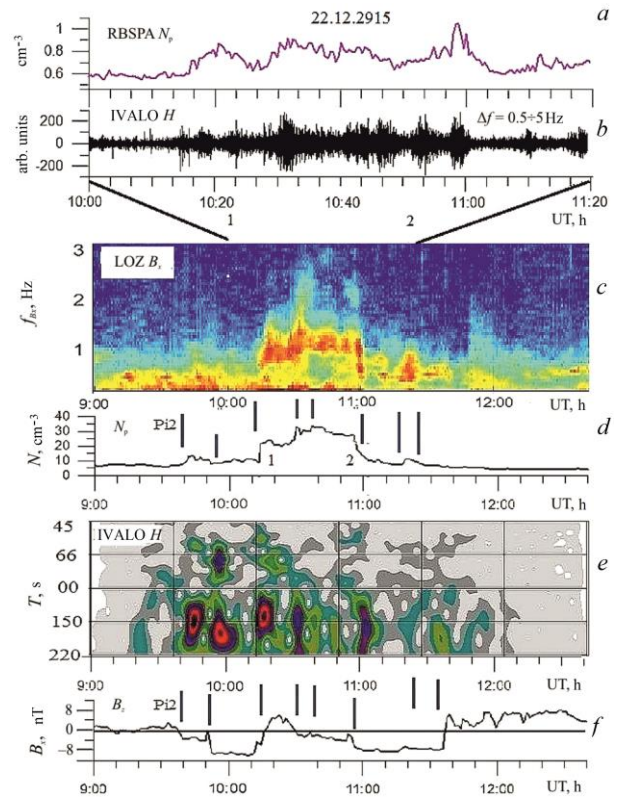Examine features of the pulsations in the frequency

Figure 7. A DS-generated substorm in geomagnetic pulsations during near noon hours: partial proton density from the RBSPA satellite (*a*); variation in the intensity of geomagnetic pulsations in the frequency range 0.5–5 Hz (*b*); spectrogram of Pc1 high-frequency geomagnetic pulsations (IPDP) at the observatory Lovozero (*c*); SW proton density variation in DS (*d*); spectrogram of geomagnetic pulsations in the frequency range 45–220 s at the observatory Ivalo (*e*); variation in IMF B_z (*f*). Vertical lines mark the intervals of correspondence between the SW proton density increase and the IPDP generation (*c*, *d*) and correspondence of the Pi2 generation when B_z passes through 0 (*e*, *f*). Numbers 1 and 2 indicate the correspondence of the intervals of increasing SW proton density with variations in the partial proton density in the magnetosphere at a distance of $\sim 5R_E$ and in the geomagnetic pulsation intensity

range 0.5–5 Hz (Figure 7, *b*, *c*). Figure 7, *c* depicts Pc1 pulsations with a nonstationary spectrum. The spectrum exhibits regions of the frequency increase and decrease that coincide in time with the increase and decrease in the SW plasma density in the DS. In addition, the pulsation amplitude envelope (Figure 7, *b*) is modulated by variations in the partial proton density in the magnetosphere (Figure 7, *a*). In [Yahnina et al., 2008; Yakhnin et al., 2019], the cyclotron instability of ring current ions stimulated by pulse compression of the magnetosphere by SW pressure jumps was considered as a source of such pulsations. However, pay attention to the features of the oscillation spectra that by morphological characteristics are close to radiation with a nonstationary spectrum of the IPDP type, associated with cyclotron instability of protons injected into the radiation belt during substorms during pre-midnight hours [Kangas et al., 1998].

Let us investigate the phenomena that occur in the magnetotail. Observations of plasma and magnetic field

parameters from the THB, THC and THA, THD, and THE satellites allow us to trace the motion and transformation of the December 22, 2015 DS to distances of ~44.5R_E and ~11.4R_E respectively. Let us note an important detail — the DS penetrates into the magnetosheath, affects the magnetosphere, and after ~15 min it is successively observed by the THB, THC satellites in the magnetosheath (~44.5 R_E) and, in a deformed form, by the THA, THD, THE satellites in the central part of the magnetotail plasma sheet (~11.4 R_E).

Figure 8 gives details on the DS dynamics. A noteworthy fact is the preservation of the structure and time scales of the DS and the anticorrelation between the *B* and N_p profiles when DS moves from the WIND satellite (~200R_E) to Earth and penetrates into the magnetosheath at distances up to ~44.5R_E (Figure 8 *a*, *b*). In the vicinity of the magnetotail plasma sheet at a distance of ~10R_E (THE), the picture changes dramatically. The structures observed are no longer DS since there is no anticorrelation between *B* and N_p (Figure 8, *c*). In this case, N_p decreases almost by a factor of ten (compared to the magnetosheath), and *B* increases about five times. All this presumably reflects the dissipative processes initiated by the impact of DS on magnetized plasma of the magnetotail.

4. MAIN RESULTS

1. The DS–magnetosphere interaction after a long period of northward B_z orientation generates an isolated global substorm whose duration depends on the duration of the interaction. The substorm begins around noon due to the DS impact on the magnetosphere and propagates eastward. The substorm is triggered by a sharp change in B_z direction.

2. All phases of the substorm are observed for two hours — the growth, expansion, and recovery phases — which are determined by the combined effect of variations in the SW plasma density and abrupt changes in the direction of the IMF vertical component.

3. Compression of the magnetosphere leads to proton precipitation at a distance of ~5R_E and excitation of cyclotron instability in the radiation belt, which is reflected in the generation of Pc1 pulsations (IPDP) in a large latitude-longitude range during the near noon hours.

4. The DS passes into the magnetosphere, and its effect is observed in the magnetosheath and plasma sheet of the magnetotail.

Our results and the results of studies of the DS–magnetosphere interaction reported in [Parkhomov et al., 2015, 2020, 2021] can be explained by the model [McPherron et al., 1986] presented in Figure 9, *a*. The model was built on the basis of a large statistics of observations of global isolated substorms, which were triggered by a sharp change in the long-term (~2 hrs) northward orientation of IMF_{Bz} to the southward. The substorms were determined from a sharp steady decrease in the *AL* index, which coincided with the onset of Pi2 geomagnetic pulsations. The top panel of Figure 9, *a* illustrates changes in the IMF vertical component. The middle panel illustrates an SW pressure change;
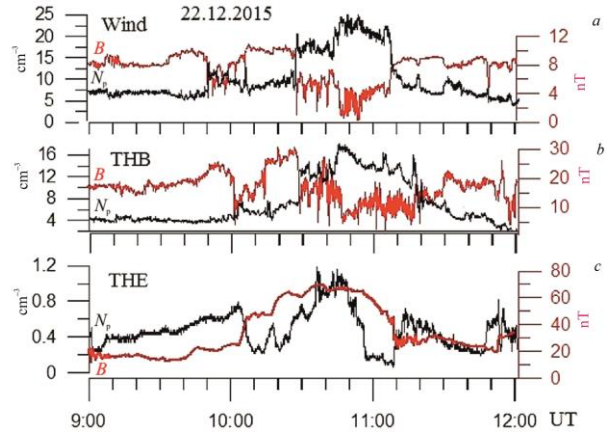

Figure 8. Variations in the magnetic field strength modulus *B* (black curve) and proton density N_p (red curve): *a* — in the solar wind according to WIND satellite data; *b* — in the magnetosheath according to THB satellite data; *c* — in the magnetosphere according to THE satellite data

the bottom panel, variations in the *AL* index of the westward electrojet during the isolated substorm. The bottom panel of Figure 9, *a* shows schematically the development of the substorm. It is important to stress that the onset of the substorm is associated with a sharp turn of IMF_{Bz} to the south (red vertical line). Also noteworthy is that the substorm phases in the model are defined by the simultaneous change in IMF and SW pressure. Stages of the substorm development are numbered 1–7 in Figure 9.

Let us turn now to Figure 9, *b*, where the same IMF parameters are presented, but the proton density is taken instead of the SW pressure. Since the SW velocity in the event considered remains constant (410±12 km/s), the SW pressure variation will be determined by the density variation. Instead of the auroral magnetic activity index *AL* used in the papers cited, we employ the global *SML* index and the local *IL* index calculated by the same method as *AL*.

Figure 9, *a*, *b* shows an amazing coincidence of details 1–7 in the model and the global isolated substorm generated by the interaction between the December 22, 2015 DS of slow SW and the magnetosphere. According to [Hsu, McPherron, 2003], a similar pattern is observed in 44 % of isolated substorms. Parkhomov et al. [2020] indicate that 24 % of isolated substorms are connected with DS in slow SW. However, the effects of the DS–magnetosphere interaction, as shown in [Parkhomov et al., 2021], are the same for slow and sporadic SW, which can bring our statistics closer to the statistics obtained in [Hsu, McPherron, 2003].

V.A. Parkhomov, V.G. Eselevich, M.V. Eselevich, B. Tsegmed, S.Yu. Khomutov, Tero Raita, G.V. Popov, A.A. Mochalov, S.V. Pilgaev, R.A. Rakhmatulin
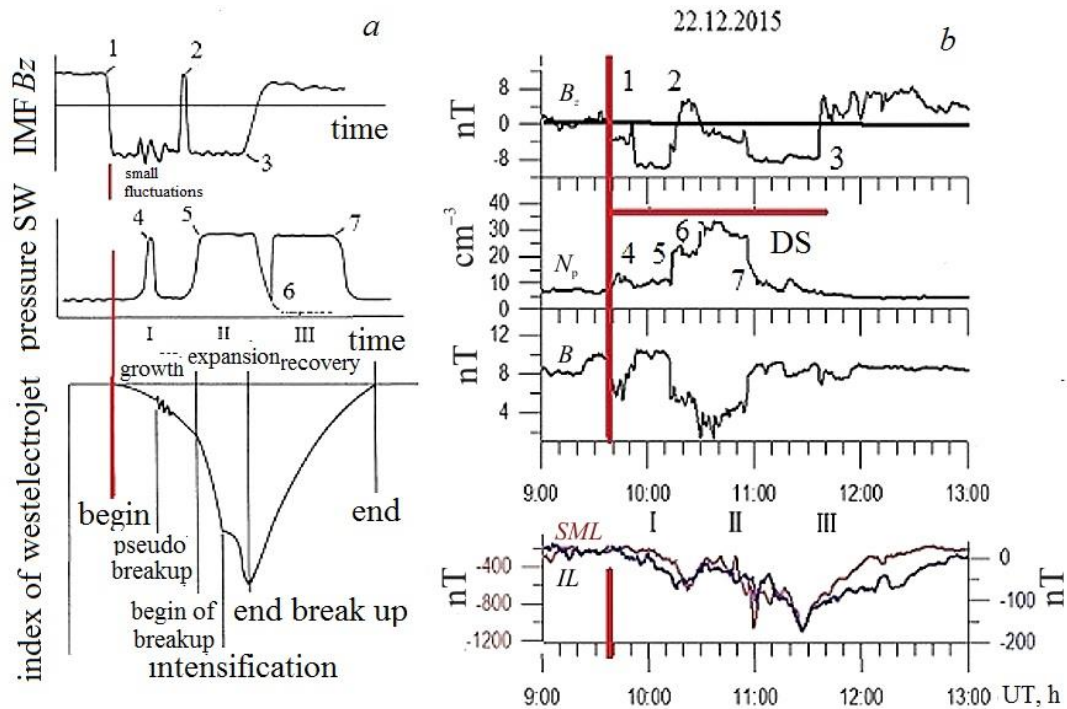
Figure 9. Statistical model of the relationship between variations in SW and IMF parameters during an isolated substorm (*a*, from top to bottom): IMF B_z, SW pressure, and *AL* index. Variations in SW and IMF parameters during the December 22, 2015 isolated substorm (*b*, from top to bottom): vertical component B_z, SW proton density N_p, IMF strength modulus, *SML* and *IL* indices. Arabic numerals denote characteristic moments of the substorm (see Figure 1 from [McPherron et al., 1986]); Roman numerals designate the substorm phases

REFERENCES

Akasofu S.-I. Auroral substorms: Search for processes causing the expansion phase in terms of the electric current approach. *Space Sci Rev*. 2017, vol. 212. pp. 341–381. DOI: 10.1007/s11214-017-0363-7.

Borrini G., Wilcox J.M., Gosling J.T., Bame S.J., Feldman W.C. Solar wind helium and hydrogen structure near the heliospheric current sheet; a signal of coronal streamer at 1 AU. *J. Geophys. Res*. 1981, vol. 86, p. 4565.

Dmitriev A.V., Suvorova A.V. Large-scale jets in the magnetosheath and plasma penetration across the magnetopause: THEMIS observations. *J. Geophys. Res.: Space Phys*. 2015, vol. 120, iss. 6. DOI: 10.1002/2014JA020953.

Echim M.M., Lemaire J.F. Laboratory and numerical simulations of the impulsive penetration mechanism. *Space Sci. Rev*. 2000, vol. 92, pp. 56–601.

Eselevich V.G. Solar flares: geoeffectiveness and the possibility of a new classification. *Planet. Space Sci*. 1990, vol. 38, iss. 2, pp. 189–206. DOI: 10.1016/0032-0633(90)90083-3.

Eselevich V.G., Fainshtein V.G. The heliospheric current sheet (HCS) and high-speed solar wind: interaction effects. *Planet. Space Sci*. 1991, vol. 39, pp. 737–744. DOI: 10.1016/0032-0633(91)90163-5.

Eselevich M.V., Eselevich V.G. Fractal structure of the heliospheric plasma sheet at the Earth's orbit. *Geomagnetizm i aeronomiya* [Geomagnetism and Aeronomy]. 2005, vol. 45, no. 3, pp. 326–336.

Eselevich V.G., Fainshtein V.G., Rudenko G.V. Study of the structure of streamer belts and chains in the solar corona. *Solar Phys*. 1999, vol. 188, pp. 277–297. DOI: 10.1023/A:1005216707272.

Eselevich M., Eselevich V., Fujiki K. Streamer belt and chains as the main sources of quasi-stationary slow solar wind. *Solar Phys*. 2007, vol. 240, pp. 135–151. DOI: 10.1007/s11207-006-0197-z.

Gjerloev J.W. The SuperMAGdata processing technique. *J. Geophys. Res*. 2012, vol. 117, iss. A9, A09213. DOI: 10.1029/2012JA017683.

Hsu T.-S., McPherron R.L. Occurrence frequencies of IMF triggered and nontriggered substorms. *J. Geophys. Res*. 2003, vol. 108, iss. A7, 1307. DOI: 10.1029/2002JA009442.

45

Kangas J., Guglielmi A., Pokhotelov O. Morphology and physics of short-period magnetic pulsations (A Review). *Space Sci. Rev*. 1998, vol. 83, pp. 435–510. DOI: 10.1023/A: 1005063911643.

Karlsson T., Kullen A., Liljeblad E., Brenning N., Nilsson H., Gunell H., Hamrin M. On the origin of magnetosheath plasmoids and their relation to magne-tosheath jets. *J. Geophys. Res.: Space Phys*. 2015, vol. 120, iss. 9, pp. 7390–7403. DOI: 10.1002/2015JA021487.

Katsavriasi C., Rapits S., Daglis L.A., Karlsson T., Georgiou M., Balasis G. On the generation of Pi2 pulsations due to plasma flow patterns around magnetosheath jets. *Geophys. Res. Lett.* 2021, vol. 48, iss. 15, e2021GL093611. DOI: 10.1029/ 2021GL093611.

Kepko L., McPherron R.L., Amm O., Apatenkov S., Baumjohann W., Birn J., Lester M., Nakamura R., Pulkkinen T.I., Sergeev V. Substorm current wedge revisited. *Space Sci. Rev.* 2015, vol. 190, pp. 1–46. DOI: 10.1007/s11214-014-0124-9.

Lemaire J., Roth M. Differences between solar wind plasmoids and ideal magnetohydrodynamic filaments. *Planet. Space Sci*. 1981, vol. 29, iss. 8, pp. 843–849.

McPherron R.L., Terasawa T., Nishida A.J. Solar wind triggering of substorm expansion onset. *J. Geomag. Geoelectr.* 1986, vol. 38, iss. 11, pp. 1089–1108. DOI: 10.5636/jgg.38.1089.

Nishida A. *Geomagnitnyi diagnoz magnitosfery* [Geomagnetic Diagnosis of the Magnetosphere]. M.: Mir, 1980, 222 p. (In Russian).

Parkhomov V.A., Borodkova N.L., Eselevich V.G., Eselevich M.V. Abrupt changes of density in sporadic solar wind and their effect on Earth magnetosphere. *Cosmic Research*. 2015, vol. 53, no. 6, pp. 411–422. DOI: 10.1134/S0010952515050093.

Parkhomov V.A., Borodkova N.L., Eselevich V.G., et al. Solar wind diamagnetic structures as a source of substorm-like disturbances. *J. Atmos. Solar-Terr. Phys.* 2018, vol. 181, pp. 55–67. DOI: 10.1016/j.jastp.2018.10.010.

Parkhomov V.A., Eselevich V.G., Eselevich M.V., Dmitriev A.V., Suvorova A.V., Vedernikova T.I. Classification of magnetospheric responses to interaction with diamagnetic structures of slow solar wind. *Solar-Terr. Phys*. 2020, vol. 6, iss. 4, pp. 24–36. DOI: 10.12737/stp-64202004.

Parkhomov V.A., Eselevich V.G., Eselevich M.V., Dmitriev A.V., Suvorova A.V., Khomutov S.Yu., Tsegmed B., Tero Raita. Magnetospheric response to the interaction with the sporadic solar wind diamagnetic structure. *Solar-Terr. Phys*. 2021, vol. 7, iss. 3, pp. 11–28. DOI: 10.12737/stp-73202102.

Pneuman G.W. Ejection of magnetic fields from the sun-Acceleration of a solar wind containing diamagnetic plasmoids. *Astrophys. J*. 1983, vol. 265, pp. 468–482.

Rakhmatulin R.A., Parkhomov V.A., Lukovnikova V.I. On the appearance of Pi pulsations in the preliminary phase of a substorm. *Magnitosfernye issledovaniya* [Magnetosphere research]. 1984, no. 5, pp. 111–120. (In Russian.)

Saito T. Geomagnetic pulsations. *Space Sci. Rew*. 1969. vol. 10, iss. 3, pp. 319–412.

Schwenn R., Dal Lago A., Huttunen E., Gonzalez W.D. The association of coronal mass ejections with their effects near the Earth. *Ann. Geophys*. 2005, vol. 23, pp. 1033–1059. DOI: 10.5194/angeo-23-1033-2005.

Svalgaard L.J., Wilcox W., Duvall T.L. A model combining the solar magnetic field. *Solar Phys.* 1974, vol. 37, p. 157.

Troshichev O.A., Janzhura A. *Space Weather Monitoring by Ground-Based Means: PC Index*. Springer-Verlag, 2012, 287 p. DOI: 10.1007/978-3-642-16803-1.

Vorobjev V.G., Antonova E.E., Yagodkina O.I. How the intensity of isolated substorms is controlled by the solar wind parameters. *Earth, Planets and Space.* 2018, vol. 70, p. 148. DOI: 10.1186/s40623-018-0922-5.

Wang Y.M., Sheeley N.R., Rich N.B. Coronal pseudo-streamers. *Astrophys. J.* 2007, vol. 685, no. 2. pp. 1340–1348. DOI: 10.1086/511416.

Yahnin A.G., Titova E.E., Demekhov A.G., Yahnina T.A., Popova T.A., Lyubchich A., Manninen J., Raita T. Simultaneous observations of EMIC waves, ELF/VLF waves, and energetic particle precipitation during multiple compressions of the magnetosphere. *Geomagnetism and Aeronomy*. 2019, vol. 59, iss. 6, pp. 668–680. DOI: 10.1029/2008JA013099.

Yahnina T.A., Frey H.U., Bösinger T., Yahnin A.G. Evidence for subauroral proton flashes on the dayside as the result of the ion cyclotron interaction. *J. Geophys. Res.: Space Phys.* 2008, vol. 113, iss. A7. DOI: 10.1029/2008JA013099.

URL: https://space.fmi.fi/image/www/index.php?page=il_index (accessed February 15, 2022).

URL: http://carisma.ca/carisma-data/fgm-auroral-indici (accessed February 15, 2022).

URL: http://cdaweb.gsfc.nasa.gov/cgi-bin/eval2.cgi (accessed February 15, 2022).

URL: http://wdc.kugi.kyoto-u.ac.jp/dst_provisional/201512/index.html (accessed February 15, 2022).

URL: http://www.obsebre.es/en/rapid (accessed February 15, 2022).

URL: https://cdaw.gsfc.nasa.gov/CME_list (accessed February 15, 2022).

URL: http://bdm.iszf.irk.ru (accessed February 15, 2021).

URL: http://spaceweather.ru/ru/node/32 (accessed February 15, 2022).

URL: http://ckp-rf.ru/ckp/3056 (accessed February 15, 2022).

How to cite this article
Parkhomov V.A., Eselevich V.G., Eselevich M.V., Tsegmed B., Khomutov S.Yu., T. Raita, Popov G.V., Mochalov A.A., Pilgaev S.V., Rakhmatulin R.A. Correspondence of a global isolated substorm to the McPherron statistical model. *Solar-Terrestrial Physics*. 2022. Vol. 8. Iss. 2. P. 37–46. DOI: 10.12737/stp-82202206.